

On the road to precision cosmology with high redshift HII galaxies^{*}

R. Terlevich,^{1,2†} E. Terlevich,¹ J. Melnick,^{3,8} R. Chávez,¹ M. Plionis,^{4,1,5} F. Bresolin,⁶ and S. Basilakos.⁷

¹*Instituto Nacional de Astrofísica Óptica y Electrónica, AP 51 y 216, 72000, Puebla, México.*

²*Institute of Astronomy, University of Cambridge, Madingley Road, Cambridge CB3 0HA, UK.*

³*European Southern Observatory, Alonso de Cordova 3107, Santiago, Chile.*

⁴*Physics Dept., Aristotle Univ. of Thessaloniki, Thessaloniki 54124, Greece*

⁵*National Observatory of Athens, P. Pendeli, Athens, Greece*

⁶*Institute for Astronomy of the University of Hawaii, 2680 Woodlawn Drive, 96822 Honolulu, HI USA.*

⁷*Academy of Athens, Research center for Astronomy and Applied Mathematics, Soranou Efessiou 4, 11527, Athens, Greece.*

⁸*Observatorio Nacional, Rua José Cristino 77, 20921-400 Rio de Janeiro, Brasil.*

v2.01 — Compiled at 2:22 hrs on 4 March 2022

ABSTRACT

We report the first results of a programme aimed at studying the properties of high redshift galaxies with on-going massive and dominant episodes of star formation (HII galaxies). We use the $L(\text{H}\beta) - \sigma$ distance estimator based on the correlation between the ionized gas velocity dispersions and Balmer emission line luminosities of HII galaxies and Giant HII regions to trace the expansion of the Universe up to $z \sim 2.33$. This approach provides an independent constraint on the equation of state of dark energy and its possible evolution with look-back time.

Here we present high-dispersion (8,000 to 10,000 resolution) spectroscopy of HII galaxies at redshifts between 0.6 and 2.33, obtained at the VLT using XShooter. Using six of these HII galaxies we obtain broad constraints on the plane $\Omega_m - w_0$. The addition of 19 high- z HII galaxies from the literature improves the constraints and highlights the need for high quality emission line profiles, fluxes and reddening corrections. The 25 high- z HII galaxies plus our local compilation of 107 HII galaxies up to $z = 0.16$ were used to impose further constraints. Our results are consistent with recent studies, although weaker due to the as yet small sample and low quality of the literature data of high- z HII galaxies.

We show that much better and competitive constraints can be obtained using a larger sample of high redshift HII galaxies with high quality data that can be easily obtained with present facilities like KMOS at the VLT.

Key words: H II galaxies – distance scale – cosmology: observations

1 INTRODUCTION

HII galaxies (HIIG) are most extreme narrow emission line star forming systems selected from spectroscopic surveys as those having the largest equivalent widths (EW) in their emission lines, i.e. $\text{EW}(\text{H}\beta) > 50\text{\AA}$ (or $\text{EW}(\text{H}\alpha) > 200\text{\AA}$) in their rest frame and being extremely compact. The lower limit required in the selected equivalent width of the re-

combination hydrogen lines is of fundamental importance to guarantee that the sample of HIIG is composed by systems in which a single and very young starburst, less than 5 Myr in age, dominates the total luminosity output. This selection criterion also minimizes the possible contamination by an underlying older population or older clusters inside the spectrograph aperture (cf. Melnick, Terlevich & Terlevich 2000; Dottori 1981; Dottori & Bica 1981; Chávez et al. 2014) and the ionizing photon escape. HIIG thus selected are spectroscopically indistinguishable from young Giant Extragalactic HII Regions (GEHRs) in nearby galaxies (e.g. 30 Doradus in the LMC or NGC 604 in M33). This is highlighted by the

^{*} Partly based on observations obtained at the European Southern Observatory, programme ID 091.A-0413(A)

[†] E-mail: rjt@inaoep.mx & rjt@ast.cam.ac.uk

fact that when discovered, the prototypical HIIG I Zw18 and II Zw40 were named “Isolated Extragalactic H II regions” (Sargent & Searle 1970). On the other hand, the compactness requirement biases the sample towards single bursts with relatively small crossing times.

Under the working hypothesis of instantaneous coeval star formation (ISF) it is possible to define an age for the stellar population. Even if continuous star formation (CSF) is assumed and a wide range of stellar ages is present the ionization will be dominated by the stars born in the last 5 Myrs. Thus from this point of view not much difference is expected in the observables of these extreme emission line starbursts between the instantaneous and the continuous case. There are parameters however that will differ like the EW of the IR-CaII triplet or the total $L(\text{H}\alpha)/\text{Mass}$ relation. Another important difference is that in the case of CSF one expects to detect the WR features in all systems while for ISF they are expected only in a fraction of them.

The optical properties of HIIG can be considered as those of a “naked” extremely young and compact burst of star formation rather than those of the host galaxy.

It has been shown that GEHR and HIIG exhibit a tight correlation between the luminosity and the width of their emission lines, the $L(\text{H}\beta) - \sigma$ relation (Terlevich & Melnick 1981). The scatter in this relation is small enough that it can be used to determine cosmic distances independently of redshift (see Terlevich & Melnick 1981; Melnick, Terlevich & Moles 1988; Melnick, Terlevich & Terlevich 2000; Fuentes-Masip et al. 2000; Telles 2003; Bosch, Terlevich & Terlevich 2002; Siegel et al. 2005; Bordalo & Telles 2011; Chávez et al. 2012, 2014). HIIG can reach $\text{H}\beta$ luminosities larger than $10^{42} \text{ erg s}^{-1}$ making them observable even at relatively large redshifts ($z > 3$) with present-day NIR spectrographs.

In (CSF) we showed that the $L(\text{H}\beta) - \sigma$ relation constitutes a viable alternative to SNe Ia for the determination of cosmological parameters and presented a general strategy to use high z HIIG as effective cosmological probes to reduce significantly the parameter space of the dark energy equation of state and test its possible evolution with redshift.

To date, the cosmic acceleration has been traced directly only by means of SNe Ia and up to redshift $z \sim 1.5$ (Riess et al. 1998; Perlmutter et al. 1999; Amanullah et al. 2010; Hicken et al. 2009; Suzuki et al. 2012), a fact which implies that it is important to use alternative probes at higher redshifts in order to verify the SNe Ia results and to obtain more stringent constraints in the cosmological parameters solution space, with the ultimate aim of discriminating among the various theoretical alternatives which attempt to explain the accelerated expansion of the Universe (cf. Suyu et al. 2012).

In this paper we demonstrate the feasibility of using HIIG as competitive cosmological tracers to high- z thanks to the availability in 8m class telescopes of highly efficient near infrared high spectral resolution spectrographs.

We would like to reinforce what we consider a central point. The fact that a $L(\text{H}\beta) - \sigma$ relation exists at all, means that it can be used, empirically, as a distance estimator up to large redshifts, regardless of the physics that causes it. This aspect has been discussed in the literature (among others Terlevich & Melnick 1981; Melnick, Terlevich & Moles 1988; Tenorio-Tagle, Munoz-Tunon & Cox 1993; Terlevich 1997; Melnick, Tenorio-Tagle & Terlevich 1999; Melnick, Terlevich

& Terlevich 2000; Zaragoza-Cardiel et al. 2015) and will be discussed still further as more and better data becomes available.

In §2 we present the observations and data reduction, and the data (both ours and from the literature) are analysed in §3. The results are discussed in §4 and conclusions and plans for future work are given in §5.

2 OBSERVATIONS AND DATA REDUCTION

High spectral resolution spectroscopic observations were obtained using the XShooter spectrograph (Vernet et al. 2011) at the Cassegrain focus of the ESO-VLT (European Southern Observatory Very Large Telescope) in Paranal, Chile during the nights of 29 and 30 September 2013¹. We obtained spectra for the three arms using a 0.6 arcsec slit, the typical spectral resolution on the VIS arm was ~ 10000 , whereas in the NIR arm it was ~ 8000 . Total exposure times per object ranged between 1 and 3 hours.

A sample of 9 star forming galaxies with rest frame equivalent width (EW) of $\text{H}\beta > 50 \text{ \AA}$ or $\text{EW}(\text{H}\alpha) > 200 \text{ \AA}$ was selected from Hoyos et al. (2005); Erb et al. (2006a,b) and Matsuda et al. (2011). The redshift range covered was $0.64 \leq z \leq 2.33$. The observation parameters are detailed in Table 1.

A narrow slit was needed to achieve the required resolution but when combined with the excellent seeing resulted in pointing problems associated with the fact that these are faint and almost stellar objects. All pointings were blind and we had to rely on our differential astrometry. This proved to be correct, i.e. inside 0.2 arcsec in all cases but one. The narrow slit has another negative effect in the sense that slight offsets or seeing becoming worse than the slit size result in light losses. These aspects highlight the importance of spectroscopy with integral field units that minimizes the astrometry problems while at the same time optimizing the light collection.

The data reduction was carried out using the XShooter pipeline V2.3.0 over the GASGANO V2.4.3 environment² using the ‘physical model mode’ reduction.

3 DATA ANALYSIS

3.1 Emission line widths

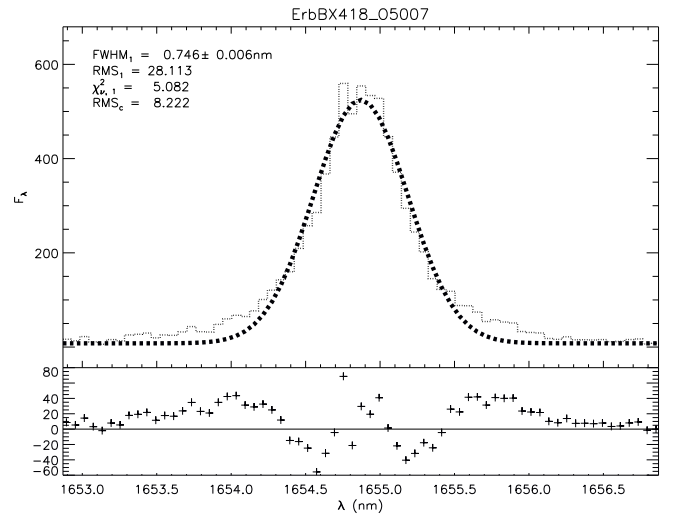
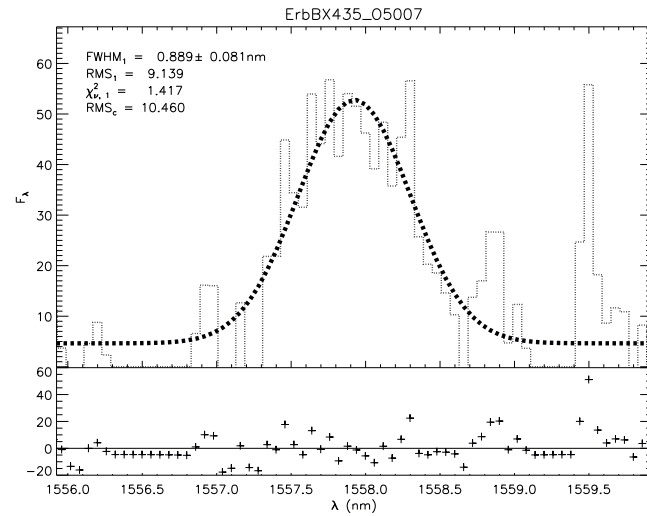
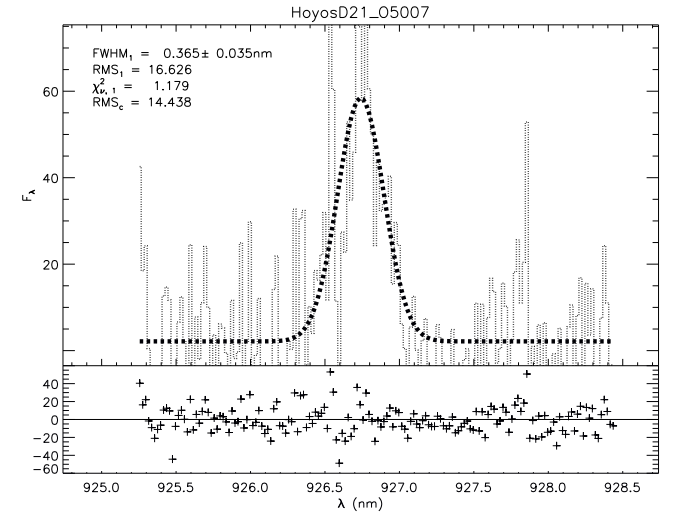
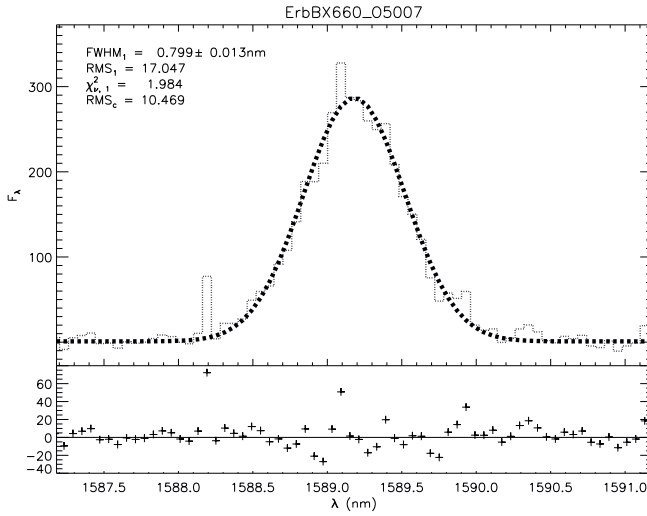
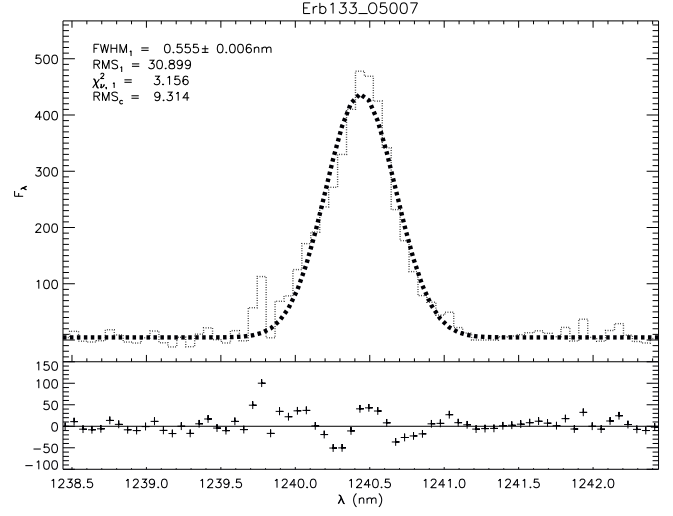
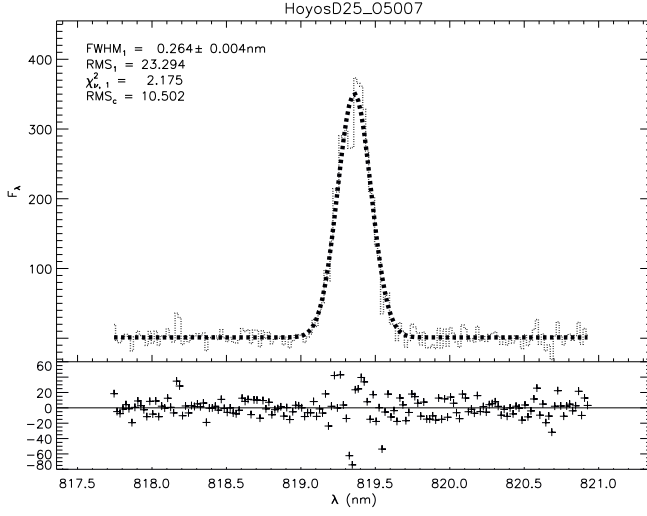
To determine the FWHM of the emission lines, single gaussians were fitted to the 1D spectral profiles of the $[\text{O III}] \lambda 5007 \text{ \AA}$ and $\text{H}\alpha$ lines when available³. These fits were performed using the IDL routine `gaussfit`. Figure 3.1 shows the fits to the $[\text{O III}] \lambda 5007 \text{ \AA}$ line.

The uncertainties of the measured FWHM were estimated using a Montecarlo analysis. A set of random realizations of every spectrum was generated using the data poissonian 1σ 1-pixel uncertainty. Gaussian fittings for every synthetic spectrum in the set were performed afterwards,

¹ Observing programme ID 60.A-9022(C)

² GASGANO is a JAVA based Data File Organizer developed and maintained by ESO.

³ Historically, $\text{H}\beta$ has been used but, when available, the stronger $\text{H}\alpha$ line is preferred



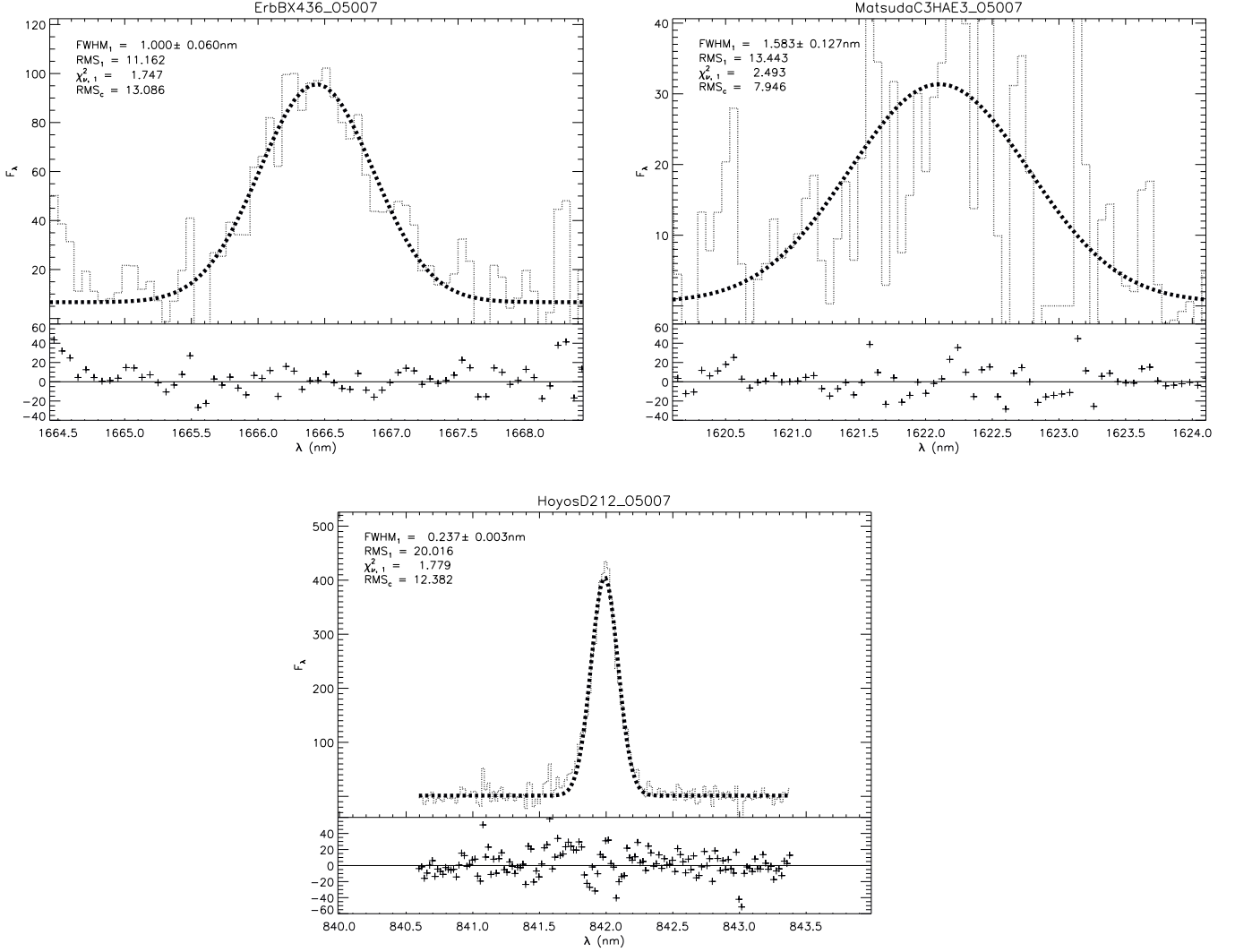


Figure 1. Gaussian fits to the [O III] $\lambda 5007$ Å line for the nine observed objects as labelled. *Upper panel:* The single gaussian fit is shown with a dashed line (thick black). The parameters of each fit are shown in the top left corner. *Lower panel:* Residuals from the fit.

and we obtained a distribution of “synthetic” FWHM from which the 1σ uncertainty for the widths measured in the spectra follows.

Table 2 lists the FWHM measurements for the high resolution observations prior to any correction such as instrumental or thermal broadening. Column (1) is the target name, column (2) is the heliocentric redshift as measured from the observed emission lines, columns (3) to (6) contain the measured central wavelength in nm and FWHM in km s^{-1} for [O III] $\lambda 5007$ and $H\alpha$ respectively.

The observed velocity dispersions (σ_o) – and their 1σ uncertainties – have been derived from the FWHM measurements of the [O III] $\lambda 5007$ Å and $H\alpha$ lines ($\sigma_o = 0.4247 \times FWHM$). Corrections for thermal (σ_{th}) and instrumental (σ_i) broadening have been applied, yielding a final velocity dispersion

$$\sigma = \sqrt{\sigma_o^2 - \sigma_{th}^2 - \sigma_i^2 - \sigma_{fs}^2} \quad (1)$$

with a spin broadening value, in the case of $H\alpha$, of $\sigma_{fs}(H\alpha) = 2.4 \text{ km s}^{-1}$ as detailed in Chávez et al. (2014).

The mean relation between the velocity dispersions of [OIII] and of $H\alpha$ [where we could measure both, including our own low- z HIIG sample from Chávez et al. (2014)] was found to be $\sigma(H\alpha) = \sigma([OIII]) + (2.91 \pm 0.31) \text{ km s}^{-1}$. We used this expression to estimate $\sigma(H\alpha)$ for those objects with only $\sigma([OIII])$ measured.

As concluded by Melnick, Terlevich & Moles (1988) and Chávez et al. (2014), imposing an upper limit to the velocity dispersion of $\log \sigma(H\beta) \lesssim 1.8 \text{ km s}^{-1}$, minimizes the probability of including rotationally supported systems. Therefore from the observed sample we selected all objects having $\log \sigma(H\alpha) < 1.8 \text{ km s}^{-1}$ thus reducing the sample to 6 objects as indicated in Table 2, column (7).

The adopted emission line velocity dispersions and their $1-\sigma$ uncertainties are shown in Table 3, column (5).

Table 1. Observing log.

(1) Name	(2) RA (J2000.0)	(3) δ	(4) date	(5) slitwidth (arcsec)	(6) exp. time VIS, NIR(sec)
HoyosD2 5	23 28 41.65	+00 18 20.0	29/9/2013	0.6	2000, 2400
Q2343-BM133	23 46 16.18	+12 48 09.3	29/9/2013	0.6	4000, 4640
Q2343-BX660	23 46 29.43	+12 49 45.5	29/9/2013	0.6	8000, 9280
HoyosD2 1	23 29 08.20	+00 20 40.7	30/9/2013	0.6	1600, 2400
Q2343-BX435	23 46 26.36	+12 47 55.1	30/9/2013	0.6	4000, 4640
Q2343-BX418	23 46 18.57	+12 47 47.4	30/9/2013	0.6	4000, 4640
Q2343-BX436	23 46 09.06	+12 47 56.0	30/9/2013	0.6	4000, 4640
MatsudaC3HAE3	02 02 37.68	+01 44 33.2	30/9/2013	0.6	4000, 4640
HoyosD2 12	02 28 45.05	+00 41 32.8	30/9/2013	0.6	3200, 4800

Table 2. Observed [O III] $\lambda 5007$ and H α central wavelength and FWHM.

(1) Name	(2) z_{hel}	(3) λ_c ([O III] $\lambda 5007$) (nm)	(4) FWHM([O III] $\lambda 5007$) (km s $^{-1}$)	(5) λ_c (H α) (nm)	(6) FWHM (H α) (km s $^{-1}$)	(7) Remarks ^a
HoyosD2 5	0.6364	819.359 \pm 0.002	96.6 \pm 1.3	1073.861 \pm 0.012	113.3 \pm 7.8	1
Q2343-BM133	1.4774	1240.440 \pm 0.003	134.1 \pm 1.5	1625.881 \pm 0.005	142.6 \pm 2.1	1
Q2343-BX660	2.1735	1589.181 \pm 0.006	150.9 \pm 2.5	2082.558 \pm 0.012	—	1
HoyosD2 1	0.8510	926.740 \pm 0.015	118.2 \pm 11.4	—	—	1
Q2343-BX435	2.1119	1557.924 \pm 0.034	171.3 \pm 15.6	2042.258 \pm 0.021	178.6 \pm 7.2	2
Q2343-BX418	2.3052	1654.870 \pm 0.002	135.3 \pm 1.0	—	—	1
Q2343-BX436	2.3277	1666.438 \pm 0.025	180.0 \pm 10.8	—	—	2
MatsudaC3HAE3	2.2397	1622.102 \pm 0.054	292.7 \pm 23.4	—	—	2
HoyosD2 12	0.6816	841.988 \pm 0.002	84.4 \pm 1.2	—	—	1

^a 1: Object used in the analysis, 2: log $\sigma > 1.8$; object not used.

3.2 Fluxes

For the objects selected from Erb et al. (2006a,b), the H α fluxes were obtained from the literature directly and we can readily deduce from the reddening corrected $f(\text{H}\alpha)$, the $f(\text{H}\beta)$ from their theoretical ratio. The three objects from Hoyos et al. (2005) do not have a direct measurement of their line fluxes; Their line luminosities were obtained using a rough estimate from their total blue luminosity and equivalent width (see Terlevich & Melnick 1981):

$$B_C = -2.5 \log[L_o(\text{H}\beta)/EW_\lambda] + 79.7, \quad (2)$$

where B_C is the absolute blue continuum magnitude, $L_o(\text{H}\beta)$ is the reddening corrected H β luminosity and EW_λ is the rest frame equivalent width of H β . These three objects have a larger uncertainty in their estimated emission line luminosities.

When available the reddening (here taken as A_V) was obtained from the literature. The A_V was derived from the published $E(B - V)$ using the value of $R_v = 4.05$ given by Calzetti et al. (2000). For those objects where the reddening was not available the mean $A_V = 0.33$ from our local sample, was adopted. We have verified that the mean values of A_V for the local and high- z samples are compatible.

The top block of table 3, column (7) shows the adopted H β fluxes and their 1σ uncertainties, after internal extinction correction, the adopted A_V values are shown in column (8).

3.3 Data from the literature

To complement the data and compare results with a larger sample (albeit of lower quality velocity dispersions) we have searched the literature for measurements of emission line FWHM of high- z HII G. Following strictly our selection criteria we were able to select a sample of 6 HII G from Erb et al. (2006a,b), 1 from Maseda et al. (2014) and 12 from Masters et al. (2014) for which $\sigma(\text{H}\alpha)$ and $f(\text{H}\alpha)$ are given, have line ratios and position in diagnostic diagrams corresponding to HII regions and $EW(\text{H}\beta) > 50\text{\AA}$ or $EW(\text{H}\alpha) > 200\text{\AA}$ plus $\text{Log } \sigma(\text{H}\alpha) < 1.8 + 1$ sigma error. Only those objects with error less than 25% in the measured velocity dispersion are included.

The lower block of Table 3 shows the data for the 19 objects selected from the literature.

4 DISCUSSION

4.1 The $L - \sigma$ relation

Taking the concordance Λ CDM cosmology as the fiducial model we calculated the distances and hence the luminosities for all the objects in our sample (see subsection 4.3). The values of the luminosities are listed in Table 3, column (6). As mentioned in section 3.1 three of the objects listed in tables 1 and 2 are not included in the analysis because they do not fulfil the selection criterion on σ .

Figure 2 shows the $L - \sigma$ relation for the 25 high- z sample of HII galaxies [6 high- z HII G observed with XShooter

Table 3. Luminosity and gas velocity dispersion of high- z H II Galaxies obtained from the literature and from observations.

(1) Name	(2) RA (J2000.0)	(3) δ	(4) z_{hel}	(5) $\log \sigma$ (km s $^{-1}$)	(6) $\log L$ (H β) (erg s $^{-1}$)	(7) f (H β) (10 $^{-17}$ erg s $^{-1}$ cm $^{-2}$)	(8) A_V	(9) W (H α) (Å)	(10) Ref.
Q2343-BM133	23 46 16.18	+12 48 09.31	1.4774	1.756 \pm 0.017	42.202 $^{+0.053}_{-0.060}$	13.069 \pm 1.293	0.20 \pm 0.14	2245	1
Q2343-BX418	23 46 18.57	+12 47 47.38	2.3052	1.758 \pm 0.016	42.041 $^{+0.038}_{-0.042}$	3.031 \pm 0.116	0.14 \pm 0.10	1639	1
Q2343-BX660	23 46 29.43	+12 49 45.54	2.1735	1.808 \pm 0.016	42.024 $^{+0.039}_{-0.043}$	3.363 \pm 0.146	0.04 \pm 0.03	488	1
HoyosD2-5	23 28 41.65	+00 18 20.00	0.6364	1.597 \pm 0.023	41.393 $^{+0.151}_{-0.233}$	16.171 \pm 6.573	0.28 \pm 0.04	96 $^a \pm 5$	2
HoyosD2-1	23 29 08.20	+00 20 40.70	0.8510	1.695 \pm 0.049	41.692 $^{+0.151}_{-0.233}$	15.803 \pm 6.424	0.28 \pm 0.04	98 $^a \pm 5$	2
HoyosD2-12	02 28 45.05	+00 41 32.80	0.6816	1.527 \pm 0.027	41.297 $^{+0.149}_{-0.230}$	10.965 \pm 4.410	0.00 \pm 0.04	110 $^a \pm 15$	2
HDF-BX1277	12 37 18.59	+62 09 55.54	2.2713	1.799 \pm 0.062	41.907 $^{+0.049}_{-0.056}$	2.305 \pm 0.201	0.29 \pm 0.09	—	1
Q0201-B13	02 03 49.25	+11 36 10.58	2.1663	1.792 \pm 0.070	41.421 $^{+0.039}_{-0.043}$	0.845 \pm 0.035	0.01 \pm 0.00	—	1
Q1623-BX215	16 25 33.80	+26 53 50.66	2.1814	1.845 \pm 0.093	41.860 $^{+0.061}_{-0.072}$	2.283 \pm 0.290	0.41 \pm 0.12	—	1
Q1623-BX453	16 25 50.84	+26 49 31.40	2.1816	1.785 \pm 0.028	42.459 $^{+0.094}_{-0.120}$	9.076 \pm 2.064	0.84 \pm 0.25	187	1
Q2346-BX120	23 48 26.30	+00 20 33.16	2.2664	1.792 \pm 0.084	41.815 $^{+0.042}_{-0.046}$	1.875 \pm 0.106	0.02 \pm 0.00	—	1
Q2346-BX405	23 48 21.22	+00 24 45.46	2.0300	1.699 \pm 0.035	42.125 $^{+0.035}_{-0.039}$	5.009 \pm 0.083	0.03 \pm 0.01	358	1
COSMOS-17839	10 00 40.96	+02 21 38.88	1.4120	1.664 \pm 0.084	41.205 $^{+0.298}_{-1.848}$	1.472 \pm 1.446	0.33 \pm 0.09	325 \pm 230	3
WISP159-134	20 56 30.91	-04 47 56.30	1.3000	1.686 \pm 0.045	41.684 $^{+0.053}_{-0.060}$	5.443 \pm 0.532	0.12 \pm 0.09	314 \pm 36	4
WISP173-205	01 55 23.64	-09 03 10.20	1.4440	1.834 \pm 0.045	41.684 $^{+0.062}_{-0.072}$	4.196 \pm 0.535	0.09 \pm 0.15	603 \pm 42	4
WISP46-75	22 37 56.48	-18 42 46.10	1.5040	1.839 \pm 0.066	41.832 $^{+0.129}_{-0.185}$	5.334 \pm 1.794	0.15 \pm 0.43	245 \pm 28	4
WISP22-216	08 52 46.29	+03 08 45.90	1.5430	1.641 \pm 0.040	41.657 $^{+0.054}_{-0.062}$	3.350 \pm 0.347	0.00 \pm 0.12	—	4
WISP64-2056	14 37 30.20	-01 50 51.40	1.6100	1.746 \pm 0.039	41.716 $^{+0.050}_{-0.056}$	3.457 \pm 0.304	0.33 \pm 0.09	—	4
WISP138-173	15 45 31.03	+09 33 30.00	2.1580	1.814 \pm 0.040	42.118 $^{+0.059}_{-0.068}$	4.245 \pm 0.504	0.33 \pm 0.09	—	4
WISP64-210	14 37 28.34	-01 49 54.40	2.1770	1.830 \pm 0.039	42.043 $^{+0.052}_{-0.059}$	3.498 \pm 0.331	0.33 \pm 0.09	—	4
WISP204-133	11 19 46.37	+04 10 30.80	2.1910	1.765 \pm 0.063	41.607 $^{+0.053}_{-0.060}$	1.262 \pm 0.126	0.00 \pm 0.00	—	4
WISP70-253	04 02 02.50	-05 37 19.50	2.2150	1.628 \pm 0.041	41.590 $^{+0.038}_{-0.042}$	1.182 \pm 0.045	0.00 \pm 0.00	—	4
WISP96-158	02 09 26.37	-04 43 29.00	2.2340	1.702 \pm 0.043	41.964 $^{+0.052}_{-0.059}$	2.742 \pm 0.259	0.33 \pm 0.09	—	4
WISP138-160	15 45 36.29	+09 34 26.70	2.2640	1.838 \pm 0.044	42.318 $^{+0.049}_{-0.055}$	5.987 \pm 0.512	0.33 \pm 0.09	—	4
WISP206-261	10 34 17.56	-28 30 49.80	2.3150	1.693 \pm 0.044	42.153 $^{+0.147}_{-0.223}$	3.880 \pm 1.525	0.91 \pm 0.49	—	4

NOTE. - Units of right ascension are hours, minutes, and seconds, and units of declination are degrees, arcminutes, and arcseconds.

References: (1) Erb et al. (2006b), (2) Hoyos et al. (2005), (3) Maseda et al. (2014) & (4) Masters et al. (2014).

a W (H β).

(red stars) and 19 high- z HIIG from the literature (green triangles)], and the local sample of GHIIR and HIIG from Chávez et al. (2014).

The result is a remarkably tight correlation that underpins the use of the $L - \sigma$ relation as a distance estimator over a wide range of distances, basically from the local group of galaxies (LMC, SMC, NGC 6822, M 33) up to at least $z \sim 2.3$.

Although here we are only considering the two dimensional $L - \sigma$ relation, we would like to point out that according to Chávez et al. (2014) by including additional observables in the $L - \sigma$ relation like the size of the ionized gas region, the equivalent width of either H β or H α and the ionized gas metallicity or the continuum colour, the scatter is substantially reduced from an rms ~ 0.35 to an rms < 0.25 . The importance of this reduction in the scatter of the distance estimator cannot be overemphasized.

4.2 The Hubble diagram

Figure 3 shows the Hubble diagram for the joint sample of local and high- z systems. The points correspond to individual HIIG; their distance moduli are obtained from:

$$\mu^{ob} = 2.5 \log L(\text{H}\beta)_\sigma - 2.5 \log f(\text{H}\beta) - 100.2 \quad (3)$$

where $L(\text{H}\beta)_\sigma$ is estimated from the $L - \sigma$ relation (Figure 2) calculated for the joint local HIIG (107 objects) and GEHR

(24 objects) samples,

$$\log L(\text{H}\beta) = (5.05 \pm 0.097) \log \sigma(\text{H}\alpha) + (33.11 \pm 0.145) \quad (4)$$

The continuous lines show the behaviour of the theoretical distance modulus with redshift computed for three different cosmological models as:

$$\mu^{th} = 5 \log D_L(\mathbf{p}, z_i) + 25, \quad (5)$$

where $D_L(\mathbf{p}, z_i)$ is the luminosity distance as calculated from a set of cosmological parameters, \mathbf{p} , and a given value of redshift, z . The red line shows the behaviour of the Concordance Λ CDM cosmology with $H_0 = 74.3$. The green line shows the trend for a cosmology with $\Omega_m = 0.3$ and $w_0 = -2.0$. The solid blue line corresponds to $\Omega_m = 1.0$ and $\Omega_\lambda = 0.0$. In all three cases $\Omega_k = 0$ i.e Universe flatness is preserved. The differential version of the Hubble diagram is shown in the bottom panel.

This is a remarkable and unique Hubble diagram in the sense that it covers a huge dynamical range with a single distance estimator. It connects galaxies in the local group to galaxies at $z \sim 2.3$, a range of almost 30 magnitudes in distance modulus or more than 5 dex in redshift.

4.3 Towards precision cosmology with HII galaxies

The most general set of cosmological parameters, assuming a flat Universe, a negligible value of the radiation density parameter Ω_r and using the Chevallier-Polarski-Linder

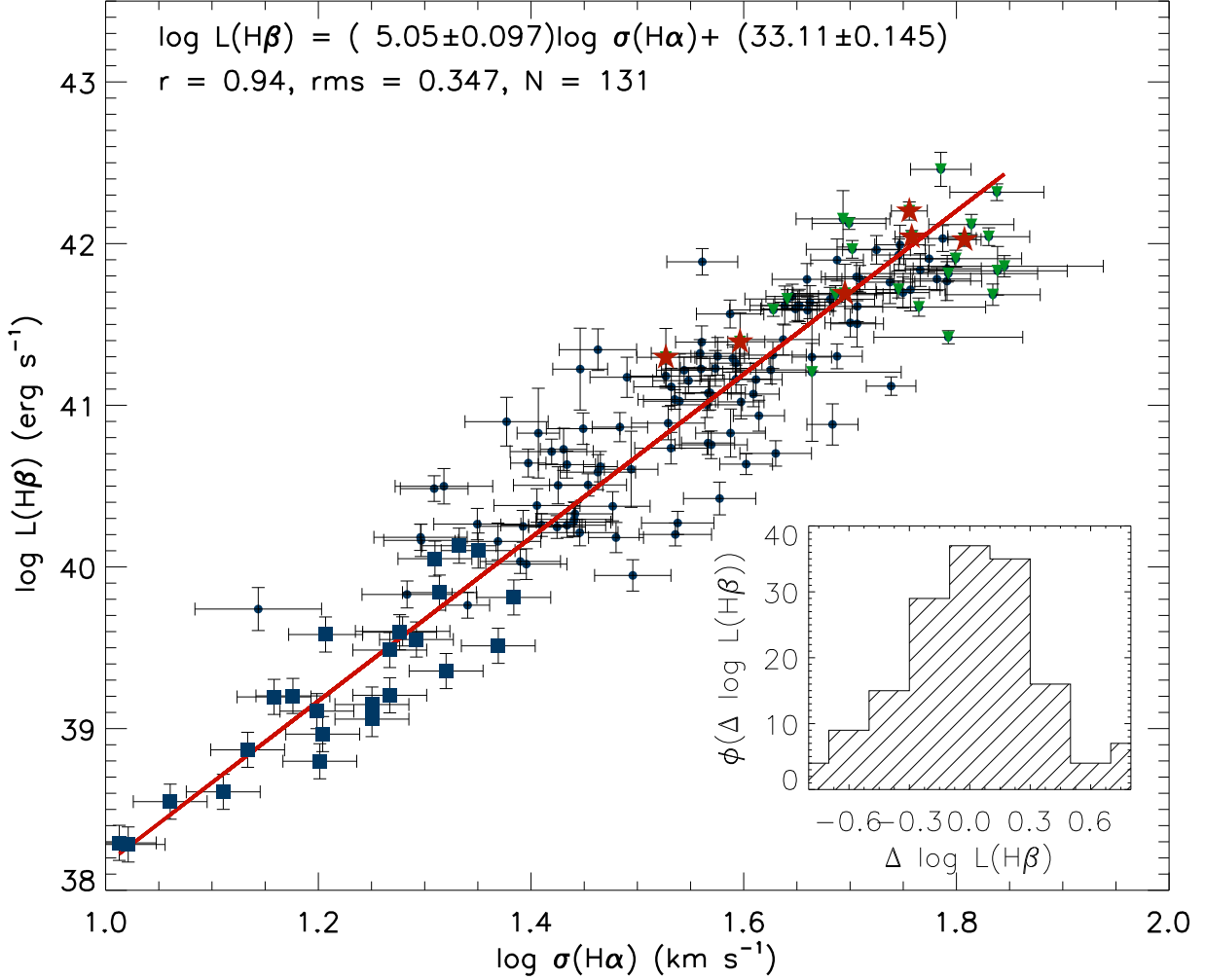


Figure 2. $L - \sigma$ relation for the combined local (131 HII and GHIIR) and high- z (25 HII) samples, the fit corresponds only to the local sample of 131 objects. Blue squares: GEHR. Blue dots: local HII. Red stars: our high- z XShooter observations. Green triangles: data from the literature. The inset shows the distribution of the residuals of the fit. The parameters of the fit are indicated at the top.

(CPL) (Chevallier & Polarski 2001; Linder 2003) model for parametrizing the value of the dark energy equation of state parameter $w(z)$, is given by $\mathbf{p} = \{H_0, \Omega_m, w_0, w_1\}$ where $w_0, w_1\}$ are the first two terms of a Taylor expansion around the present epoch, namely $w(a) = w_0 + w_1(1 - a)$ where $a = 1/(1 + z)$ is the scale factor of the Universe. In this case the luminosity distance used to estimate the value of $\mu_i^{th}(\mathbf{p}, z_i)$, is given by (cf. e.g. Weinberg 2008; Frieman et al. 2003),

$$D_L = c(1 + z) \int_0^z \frac{dz'}{H(z')} \quad (6)$$

$$H^2(z, \mathbf{p}) = H_0^2 [\Omega_m(1 + z)^3 + (1 - \Omega_m)(1 + z)^{3(1+w_0+w_1)} \times \exp\left(\frac{-3w_1z}{z+1}\right)] \quad (7)$$

To restrict the set of cosmological parameters we min-

imised the Likelihood function,

$$\chi^2(\mathbf{p}) = \sum_{i=1}^n \frac{[\mu_i^{ob}(\sigma_i, f_i) - \mu_i^{th}(\mathbf{p}, z_i)]^2}{\sigma_{\mu_i^{ob}}^2}, \quad (8)$$

$\mu_i^{ob}(\sigma_i, f_i)$ are the ‘observed’ distance moduli obtained from equation 3; σ_i are the measured velocity dispersions and f_i are the measured H β fluxes for each object. $\mu_i^{th}(\mathbf{p}, z_i)$ are the ‘theoretical’ distance moduli from equation 5 obtained from the measured redshifts by using a particular set of cosmological parameters \mathbf{p} . $\sigma_{\mu_i^{ob}}$ are their errors propagated from the uncertainties in σ_i and f_i and the slope and intercept of the distance estimator in equation 4. The summation is over the combined sample of HIIgs,

Adopting the value of $H_0 = 74.3 \pm 3.1$ obtained in Chávez et al. (2012), $w_1 = 0$ we obtain the results shown in Figure 4 for $\mathbf{p} = \{\Omega_m, w_0\}$ for the high- z sample only. Panel (a) shows the solution for the 6 high- z HII observed with XShooter; Panel (b) shows the effect of including the 19 high- z objects from the literature. It is encouraging that

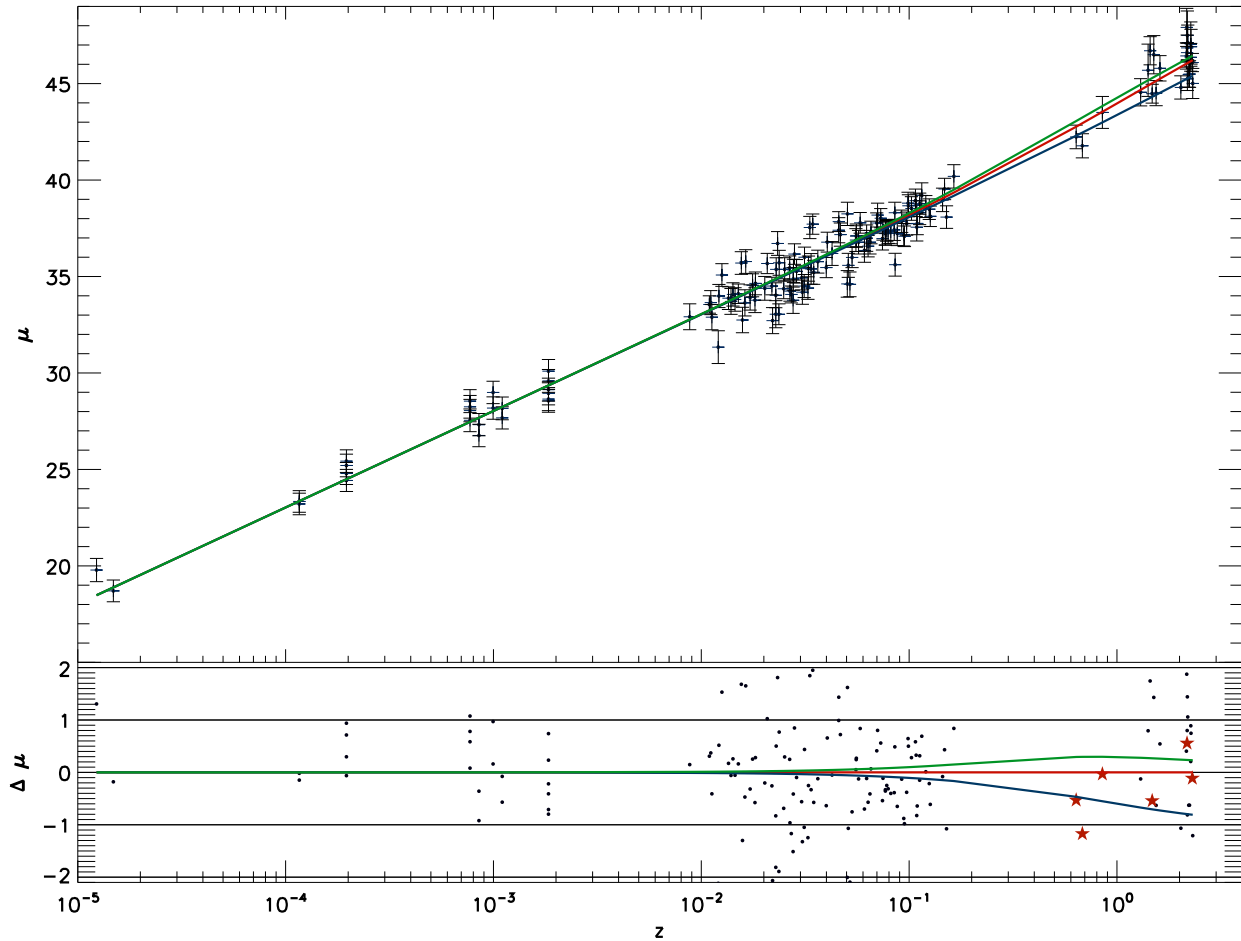


Figure 3. Hubble diagram for our sample of low and high- z HII G for three different cosmologies. The solid red line indicates the concordance Λ CDM cosmology with $\Omega_m = 0.3$; $w_0 = -1.0$ and $H_0 = 74.3$. The solid green line shows a cosmology with $\Omega_m = 0.3$ and $w_0 = -2.0$. The solid blue line corresponds to $\Omega_m = 1.0$ and $\Omega_\lambda = 0.0$. In all three cases $\Omega_k = 0$. Residuals are plotted in the bottom panel. Note the huge dynamical range in distance modulus of almost 30 magnitudes covered with the $L - \sigma$ distance estimator.

even for this small number of high- z objects we are able to restrict so much the solution space. Although the literature data are of lower quality regarding the FWHM measurements, still by adding them we are able to improve the result. This is a remarkable result considering the small number of intermediate to high- z data (just 25 objects), of which only 6 have high quality ad-hoc observations.

In Figure 5, we compare our results for the space $\mathbf{p} = \{\Omega_m, w_0\}$, joining the high- z with the local HII G samples (see left panel), with recent results from SNe Ia, CMB and BAO (right panel). The figure shows the constraints of the properties of dark energy using SNe Ia alone (Amanullah et al. 2010), the seven-year Wilkinson Microwave Anisotropy Probe data of the CMB (Komatsu et al. 2011), the position of the BAO peak from the combined analysis of the SDSS Data Release 7 and 2dFGRS data (Percival et al. 2010). The combined restrictions from SNe Ia, CMB and BAO and the measurement of the Hubble constant (H_0) from Cepheids (Riess et al. 2011) are also shown.

It is clear from the figure that our present constraints on the space $\mathbf{p} = \{\Omega_m, w_0\}$ are weaker than those for SNe Ia, but this is not surprising since in our case we have only

156 objects, most of them at $z < 0.16$ a region of space where differences between Cosmological models are almost negligible, vs. 580 SNe Ia with a maximum redshift of ~ 1.5 . The strength of our results is that our sample includes 19 objects with $z > 1.5$ where the differences between models reach maximum values.

From the comparison of the figures we can conclude first that there are no systematic shifts between the HII galaxies and SNe Ia solutions and secondly that with a larger sample of HII galaxies with high quality data it may be possible to achieve at least similar and probably even better results to those obtained with SNe Ia as found in our simulations (Plionis et al. 2011) and discussed below.

4.4 The future of the $L(\text{H}\beta) - \sigma$ distance estimator

To estimate the number of high- z tracers (N_{Hz}) required to substantially reduce the cosmological parameters solution space we used the figure of merit (FoM) as in Plionis et al. (2011). The FoM is the reciprocal area of the 2σ contour in the parameter space of any two degenerate cosmologi-

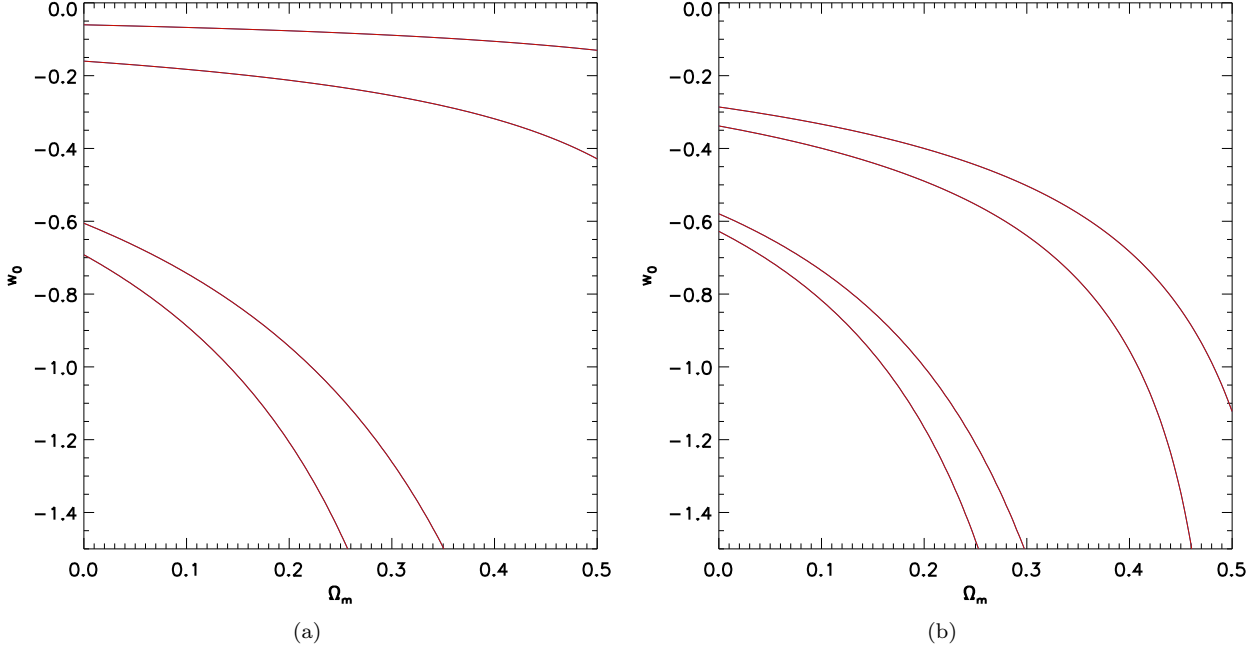


Figure 4. Solution space in the plane $\{\Omega_m, w_0\}$ (see text). Panel (a) for the 6 XShooter high- z objects. Panel (b) Same as panel (a) including 19 high- z objects from the literature. In both panels we show the 1 and 2σ contours.

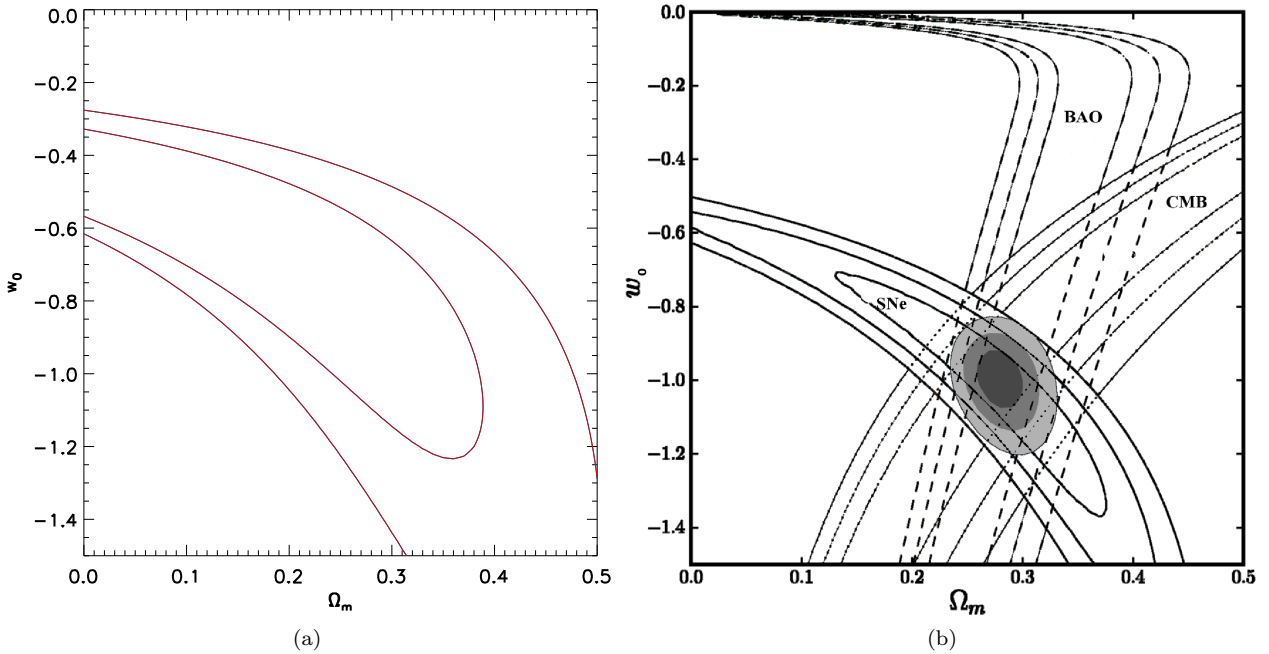


Figure 5. Comparison of restrictions on the plane $\{\Omega_m, w_0\}$ (see text). Panel (a) shows our results, obtained as described in the text for the combined 25 high- z HII and the local sample (131 HII and GHIIR). 1 and 2σ contours (random) are shown. Panel (b) after Suzuki et al. (2012) shows the recent results for 580 SNe Ia, CMB and BAOs, the 1, 2 and 3σ contours (random) are shown.

cal parameters. In this way a larger FoM indicates better restrictions to the cosmological parameters. Plionis et al. (2011) use the parameter S or “reduction factor” to compare the ratio of FoM of SNe Ia + high- z tracers to that of only SNe Ia. They found that the number of high- z tracers

needed to obtain a given S in the quintessence dark energy (QDE) model implying that w is constant but different from -1 , when combined with the intermediate and low- z SNe Ia, can be expressed as:

$$N_{Hz} \simeq 187S/S_{100} - 88 \quad (9)$$

where $S_{100} = 1.87 \log(\langle \sigma_\mu \rangle^{-1} + 0.74) + 1.28$, and $\langle \sigma_\mu \rangle$ is the mean distance modulus error for the tracer. In the case of HIIG, $\sigma_\mu \simeq 0.6$, $S_{100} \simeq 1.99$ and consequently in order to obtain a reduction of $S = 2$, we need around 100 high- z HIIG. We can visualize this in Figure 5 panel (a) for the $\mathbf{p} = \{\Omega_m, w_0\}$ plane, where a factor of 2 reduction would mean that the future 2σ contours would be similar to the present 1σ ones.

For the CPL model where w_1 is variable the same result can be expressed as:

$$N_{Hz} \simeq 404S/S_{100} - 300 \quad (10)$$

where $S_{100} = 0.49 \log(\langle \sigma_\mu \rangle^{-1} + 0.65) + 1.09$. In the case of HIIG $S_{100} \simeq 1.27$ and consequently in order to obtain a reduction of $S = 2$, about 300 high- z HIIG would be required to achieve a result similar to that obtained with present day SNe Ia samples.

5 CONCLUSIONS

We have tested the use of high redshift HIIG to trace the expansion of the Universe by means of their $L(\text{H}\beta) - \sigma$ distance estimator. To this end, we presented observations of a sample of only 9 HIIG in the redshift range of $0.6 \leq z \leq 2.3$ obtained with the ESO VLT XShooter spectrograph. After rejecting three HIIG due to either poor data or because they fall outside the selection window, we have used the remaining six to obtain constraints on the $\{H_0, \Omega_m\}$ and $\{\Omega_m, w_0\}$ planes.

The results are surprisingly good considering the small number of objects and that only two nights of XShooter time were used. The addition of 19 HIIG from the literature (albeit of poorer quality) bringing the total number of objects to 25, did improve the results and provides a clear indication of how much an increase in number can improve the constraints on the $\{H_0, \Omega_m\}$, $\{\Omega_m, w_0\}$ and $\{w_0, w_1\}$ planes.

Although our constraints are consistent with other determinations they are, as expected, definitely weaker. This is due to the small size of the intermediate to high- z sample, and the considerable uncertainties in the data taken from the literature.

Using the figure of merit approach we have estimated the expected improvement in the estimates of the cosmological parameters with a larger sample of high- z HIIG. In particular, between 100 and 300 high- z HIIG are needed to obtain a reduction in the errors of at least a factor of two. A factor of 2 reduction implies that the 2σ contours in Figure 5 panel (a) for the $\mathbf{p} = \{\Omega_m, w_0\}$ plane would be similar to the present 1σ ones and comparable to the 2σ SNe Ia contours in panel (b) that are the result of the analysis of 580 SNe Ia that took at least a decade and hundreds of nights of large telescope time to compile. In contrast, the observation of 100 HIIG can easily be achieved with multiple integrated field units instruments like VLT- KMOS, in less than thirty hours observing given the relative abundance of HIIG with a considerable number of them appearing in its 7.5 arcmin field of view.

Finally the comparison of the results of SNe Ia and HIIG will undoubtedly contribute to learning about the systematic errors that limit the precision of both empirical methods

while helping us to gain an insight into the intrinsic properties of HIIG at high redshifts. We also envisage that a substantial improvement to the present restrictions of cosmological parameters will be obtained by combining a few hundred HIIG with the SNe Ia data.

ACKNOWLEDGEMENTS

We would like to thank the ESO time allocation committee for generously awarding observing time for this project. We are indebted to Dawn Erb and Carlos Hoyos for providing all the help we needed for locating the high- z targets and are happy to acknowledge an anonymous referee whose comments helped to improve the clarity of this work. RT, ET, RC and MP are grateful to the Mexican research council (CONACYT) for supporting this research under grants CB-2005-01-49847, CB-2007-01-84746 and CB-2008-103365-F and studentship 224117. SB acknowledges support by the Research Center for Astronomy of the Academy of Athens in the context of the program “*Tracing the Cosmic Acceleration*”. The hospitality of ESO (Chile), was gratefully enjoyed specially the help from the telescope support team, Julien Girard, Petr Kabath and Andrés Pino.

REFERENCES

- Amanullah R. et al., 2010, ApJ, 716, 712
- Bordalo V., Telles E., 2011, ApJ, 735, 52
- Bosch G., Terlevich E., Terlevich R., 2002, MNRAS, 329, 481
- Calzetti D., Armus L., Bohlin R. C., Kinney A. L., Koornneef J., Storchi-Bergmann T., 2000, ApJ, 533, 682
- Chávez R., Terlevich E., Terlevich R., Plionis M., Bresolin F., Basilakos S., Melnick J., 2012, MNRAS, 425, L56
- Chávez R., Terlevich R., Terlevich E., Bresolin F., Melnick J., Plionis M., Basilakos S., 2014, MNRAS, 442, 3565
- Chevallier M., Polarski D., 2001, International Journal of Modern Physics D, 10, 213
- Dottori H. A., 1981, Ap&SS, 80, 267
- Dottori H. A., Bica E. L. D., 1981, A&A, 102, 245
- Erb D. K., Steidel C. C., Shapley A. E., Pettini M., Reddy N. A., Adelberger K. L., 2006a, ApJ, 647, 128
- Erb D. K., Steidel C. C., Shapley A. E., Pettini M., Reddy N. A., Adelberger K. L., 2006b, ApJ, 646, 107
- Frieman J. A., Huterer D., Linder E. V., Turner M. S., 2003, Phys. Rev. D, 67, 083505
- Fuentes-Masip O., Muñoz-Tuñón C., Castañeda H. O., Tenorio-Tagle G., 2000, AJ, 120, 752
- Hicken M., Wood-Vasey W. M., Blondin S., Challis P., Jha S., Kelly P. L., Rest A., Kirshner R. P., 2009, ApJ, 700, 1097
- Hoyos C., Koo D. C., Phillips A. C., Willmer C. N. A., Guhathakurta P., 2005, ApJ, 635, L21
- Komatsu E. et al., 2011, ApJS, 192, 18
- Linder E. V., 2003, Physical Review Letters, 90, 091301
- Maseda M. V. et al., 2014, ApJ, 791, 17
- Masters D. et al., 2014, ApJ, 785, 153
- Matsuda Y. et al., 2011, MNRAS, 416, 2041
- Melnick J., Tenorio-Tagle G., Terlevich R., 1999, MNRAS, 302, 677

- Melnick J., Terlevich R., Moles M., 1988, MNRAS, 235, 297
- Melnick J., Terlevich R., Terlevich E., 2000, MNRAS, 311, 629
- Percival W. J. et al., 2010, MNRAS, 401, 2148
- Perlmutter S. et al., 1999, ApJ, 517, 565
- Plionis M., Terlevich R., Basilakos S., Bresolin F., Terlevich E., Melnick J., Chavez R., 2011, MNRAS, 416, 2981
- Riess A. G. et al., 1998, AJ, 116, 1009
- Riess A. G. et al., 2011, ApJ, 730, 119
- Sargent W. L. W., Searle L., 1970, ApJ, 162, L155
- Siegel E. R., Guzmán R., Gallego J. P., Orduña López M., Rodríguez Hidalgo P., 2005, MNRAS, 356, 1117
- Suyu S. H. et al., 2012, ArXiv: astro-ph/1202.4459
- Suzuki N. et al., 2012, ApJ, 746, 85
- Telles E., 2003, in Astronomical Society of the Pacific Conference Series, Vol. 297, Star Formation Through Time, E. Perez, R. M. Gonzalez Delgado, & G. Tenorio-Tagle, ed., p. 143
- Tenorio-Tagle G., Munoz-Tunon C., Cox D. P., 1993, ApJ, 418, 767
- Terlevich R., 1997, in Revista Mexicana de Astronomia y Astrofisica, vol. 27, Vol. 6, Revista Mexicana de Astronomia y Astrofisica Conference Series, Franco J., Terlevich R., Serrano A., eds., p. 1
- Terlevich R., Melnick J., 1981, MNRAS, 195, 839
- Vernet J. et al., 2011, A&A, 536, A105
- Weinberg S., 2008, Cosmology. Oxford University Press
- Zaragoza-Cardiel J. et al., 2015, ArXiv e-prints, 1505.01497